Analysis and Comparison of a Permanent-Magnet DC Motor with a Field-Winding DC Motor

Arash Kiyoumarsi*

Abstract – The influence of magnetic saturation on electromagnetic field distribution in both a permanent-magnet direct-current (PMDC) motor and a field-winding (wound-field) direct-current (FWDC) motor, with the same output mechanical power, has been studied. In this paper, an approximate analytical method and time-stepping Finite Element Method (FEM) are used for prediction of Back-EMF and electromagnetic torque. No-load and rotor-lucked conditions, according to experimental measurements, and the FEM and analytical method studies of the motors have been considered. A sensitivity analysis has also been successfully accomplished on the major design parameters that affect motor performance. At last, these two DC motors are compared, in spite of their differences, on the basis of measured output characteristics.

Keywords: Permanent-Magnet Direct-Current (PMDC) Motor, Field-Winding (wound-field) Direct-Current (FWDC) Motor, The Finite Element Method (FEM)

1. Introduction

Prior to the development of reliable high-power solid-state switching devices, the DC motor was the dominant electric machine for all variable-speed motor drive applications. The DC motor was the most economical choice in the automotive industries for cranking motors, wind shield wiper motors, blower motors and power window motors [1].

Boules developed a two-dimensional field analysis technique by which the magnet and armature fields of both a surface–mounted brushless synchronous machine and a PMDC motor can be predicted [2,3]. In a comprehensive proposed model, Zhu et al. presented an analytical solution for predicting the resultant instantaneous magnetic field in the radially-magnetized BDCM and PMDC under any load conditions and commutation strategies [4-9].

In this paper, first, the magnetic flux density of both a six-pole, 29-slot PMDC motor and a series-exited four-pole, 21-slot FWDC motor are obtained based on an iterative analytical method. Then, the magnetic field is modeled based on a two-dimensional field analysis method considering the effect of rotor slots. The results of calculations are compared with finite element method results and predicted output characteristics of both motors are also compared with those obtained by practical output measurements with advanced equipments that are constructed for this purpose.

Section 2 introduces a brief comparison between these two different motor structures. In order to obtain flux per pole of the motors an analytical method, based on improved magnetic equivalent circuit of the motors, is briefly explained. The application of the transient finite element analysis for magnetic field calculation of these DC motors is presented in section 3. Coupled equations of magnetic field, rotor windings, and rotor motion are also presented. Section 4 contains the results of time-stepping FEM and compares them with the analytical method. In this section, the effects of screw and bolt in FWDC motor frame and magnetic holders in PMDC motor are carefully considered via taking different cross sections of the motors into account. Issues related to practical measurements are also addressed in this section. Finally, at a glimpse, a conclusion is brought in section 5.

2. Analytical Method

In Fig. 1 both the FWDC and PMDC motor structures, in which the flux lines of the mentioned motors at no-load situation are also depicted, are shown. Having determined the structure of the magnetic equivalent circuit (MEC) of the motors over one pole-pitch (Fig. 2) and electric circuit of both motors, we can specify the node permeance matrix and the node magnetic flux source vector for solving the MEC of these motors.

At the k^{th} iteration, in order to solve the magnetic equivalent circuit for unknown variables, it can be rewritten that [10]:

$$G\left(\mu_i^{(k-1)}\right) F_m^{(k)} = \Phi\left(\mu_i^{(k-1)}\right), \tag{1}$$

Where

μ_i , permeability of branch i;

$G(\mu_i)$, node permanence matrix;

F_m , vector of the node magnetic potential;

$\Phi_s(\mu_i)$, vector of the node magnetic flux source.

* Dept. of Electrical Engineering, Faculty of Engineering, University of Isfahan, Hezar Jarib Ave., Isfahan, Iran Postal code: 81746-73441, Phone: +98-311-793-4018, Fax: +98-311-793-3071
E-Mails: kiyoumarsi@eng.ui.ac.ir, kiyoumarsi_arash@yahoo.com
Received 7 January 2009; Accepted 7 July 2009

Once $F_m^{(k)}$ is solved, $\Phi(i)^{(k)}(i=1,2,...,N_b)$ can be obtained. Then, the relevant magnetic flux density $B_m^{(k)}$ is given by [10]:

$$B_m^{(k)} = \Phi(i)^{(k)} / A_i, \tag{2}$$

where Ai is the area of branch i. From the magnetization curve of the core material, the corresponding permeability $\hat{\mu}_i^{(k)}$ is obtained as [10],

$$\hat{\mu}_i^{(k)} = B_i^{(k)} / H_i^{(k)}, \tag{3}$$

where $H_i^{(k)}$ is the magnetic field intensity corresponding to $B_i^{(k)}$. Thus, the permeability for the k[th] iteration is determined by the following expression [10]:

$$\mu_i^{(k)} = \mu_i^{(k-1)} + p_i^{(k)}\left(\hat{\mu}_i^{(k)} - \mu_i^{(k-1)}\right), \tag{4}$$

in which

$$p_i^{(k)} = \min\left\{1.0, 0.01 + \frac{c_d}{c_d + \left|\hat{\mu}_i^{(k)} - \mu_i^{(k-1)}\right| / \mu_i^{(k-1)}}\right\}, \tag{5}$$

where

$p_i^{(k)}$, is the damping factor; and

c_d , is damping constant that is selected to be 0.6 here.

The above iterative process is ended when the following criterion is satisfied:

$$\left|\frac{\hat{\mu}_i^{(k)} - \mu_i^{(k-1)}}{\mu_i^{(k-1)}}\right| \le \varepsilon, \tag{6}$$

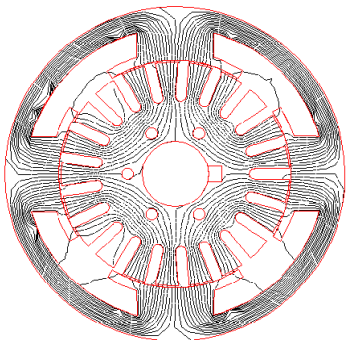

(a)

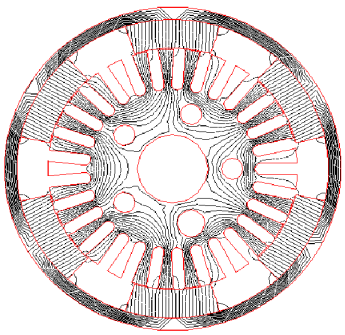

(b)

Fig. 1. Flux lines of these two DC motors at no-load condition: (a) DC and (b) PM prototype motors

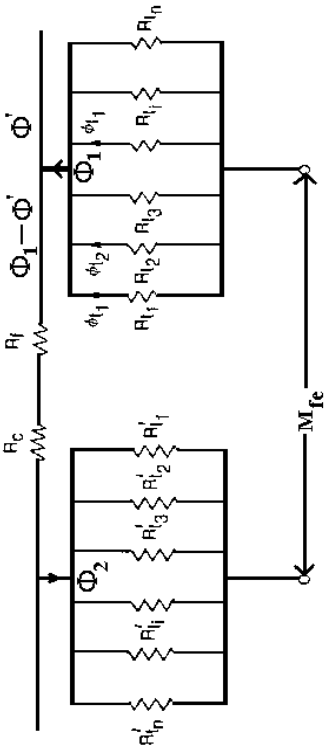

Fig. 2. Magnetic equivalent circuit of FWDC motor under one pole-pitch

where ε is the end factor determined by the accuracy requirement. Based on the solution of (1), the flux per pole characteristics of the motors are obtained.

Meanwhile these calculations, the measured B-H magnetization curve of the stator and rotor iron are taken into account. Remanent flux density of the permanent magnet (Br) and its coercive force (Hc) are considered 0.455 [T] and -260 [kA/m], respectively, according to the manufacture's data, in these simulations, for PMDC motor.

Fig. 3 shows results of this method for FWDC motor in order to determine flux per pole using the measured magnetization curves of the stator and rotor. Results of design sensitivity analysis are also evident on this Figure for changing the number of turns of the armature windings from 5 to 6 turns and 5 to 4 turns.

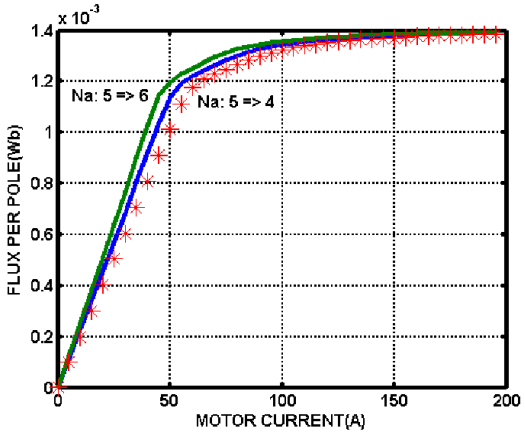

Fig. 3. Flux per pole of series-exited DC motor vs. line current

The analytical Back-EMF calculations are based on the method stated in [4-9], i.e.,

$$\psi = \sum_{n} \frac{\Phi_n}{np} K_{yn} \cos(np\alpha) , \quad (7)$$

where Φ_n and K_{yn} are defined in [4-9]. Therefore, the EMF induced in each turn of a coil is:

$$e_{turn}(t) = -\frac{d\psi}{dt} , \quad (8)$$

and the induced EMF in each coil can then be obtained as:

$$e_{coil}(t) = \sum_{n} \omega_r \Phi_{ny} K_{yn} K_{wn} N_s \sin(np\alpha), \quad (9)$$

in which Ns is the number of turns per coil and Kwn (= Kd,n*Kp,n*Kskew,n) is the n^{th} harmonic component of the winding factor.

3. Finite Element Method

3.1 Magnetic Field Model

Rotor and stator meshes are coupled together at a slip interface to allow for rotation which is a circular slip path in two-dimension in the middle of the air gap. So, there is a weak boundary condition enforced on this interface. Using Lagrange multiplier and K^{th} rotor variable, A_{rk} can be coupled to the corresponding stator variables, A_{si}, [11,15] as:

$$A_{rk} = \sum_{i=1}^{4} A_{si} N_{si}(k) . \quad (10)$$

The local virtual work method is used for torque calculation in FEM method. In the rotor PM, the magnetic field equation can be expressed as:

$$\nabla \times \nu \nabla \times A = \nu \nabla \times M . \quad 11)$$

In the rotor conductors, the magnetic field equation is given by:

$$\nabla \times \nu \nabla \times A = -J_s + \sigma \frac{\partial A}{\partial t} , \quad (12)$$

and in the rotor and stator iron regions is expressed as:

$$\nabla \times \nu \nabla \times A = 0 . \quad (13)$$

3.2 The Electrical Circuit Model [11-15]

The voltage equations of each armature coil are given by:

$$[V_{coil}] = [\frac{d}{dt}(\lambda_{coil})] + [R_{coil}] i_{coil} . \quad (14)$$

Required essential, natural and periodic boundary conditions are also considered as sets of constraint equations between nodes and elements. On the other hand, for calculation of induced Back-EMF in the FEM calculations, at first, the total flux-linkage of a coil is calculated instantaneously at one half period of the rotor revolution, as in the following equation and then the Back- EMF is determined, i.e.,

$$\lambda_{coil} = \frac{N_{coils}}{S} l_r \int Ads , \quad (15)$$

$$e_{coil}(t) = -\frac{d\lambda}{dt} . \quad (16)$$

3.3 The Mechanical System Model

Two equations of the rotation of rotor are given as follows,

$$J_{eq}(\frac{d\omega_r}{dt}) + B\omega_r = T_e - T_L , \quad (17)$$

$$\frac{d\theta_r}{dt} = \omega_r . \quad (18)$$

The above-mentioned equations are coupled in the two-dimensional circuit-field-torque coupled time stepping finite element method. This model is used to predict the produced electromagnetic torque and Back-EMF of the motors. This analysis is done by the algorithm shown in Fig. 4. At last, convergence of the procedure is checked by the velocity, magnetic vector potential and Back-EMF errors.

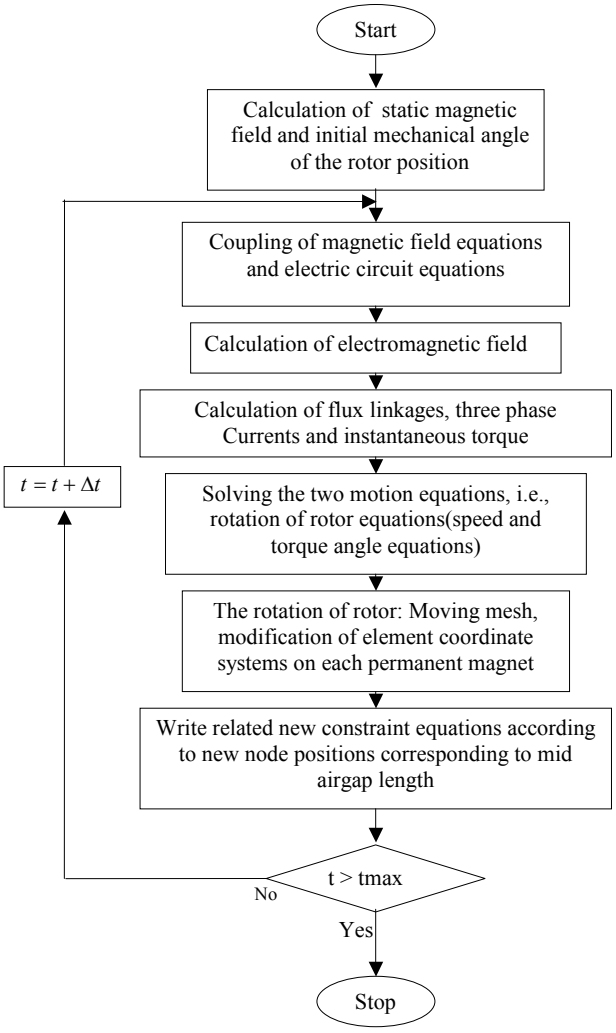

Fig. 4. Transient Finite Element Method

4. Simulation Results

Figs. 5 and 6 show the flux distribution at rated load, for the FWDC motor, and PMDC motor, respectively. Fig. 5 shows the equi-potential lines for magnetic vector potential by considering the effect of screw and bolt on the stator frame, for the FWDC motor. As it can be seen, the flux distribution under stator poles disturbs abruptly.

Fig. 6 shows the flux distribution at load with the magnetic holder, for the PMDC motor [11-15]. It can be recognized that these magnetic holders provide proper paths for the resultant flux at high armature current and do not permit high-armature reaction demagnetizing phenomenon. Their magnetic properties also are completely different from that used in the stator frame and rotor core steels.

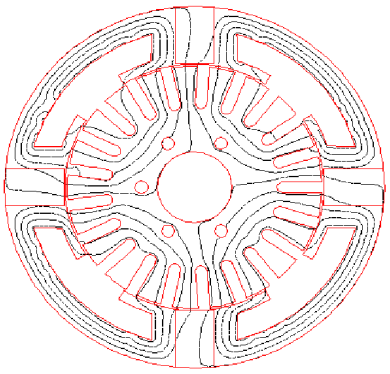

Fig. 5. Flux lines: rated-load condition; FWDC motor

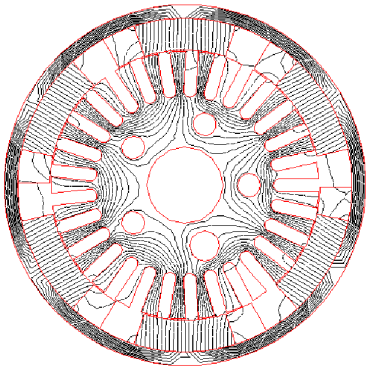

Fig. 6. Equi-potential lines for magnetic vector potential: full-load conditions; PMDC motor; magnetic holder considered

Table 1 includes the results of comparison of the FEM analysis of the FWDC motor and the two-dimensional field distribution analytical method according to average values. In this analysis, the average value of the rotor angular speed, rotor shaft torque, flux per pole, mid-airgap flux density distribution waveforms and yoke flux density distribution waveform are considered. It is notable that for these preliminary results, only the average values are considered and compared with the measured results. At the time of preparing this paper, the torque pulsations and Back-EMF accurate and precise measurements were impossible for the author because of unavailability of accurate and precise transient and dynamic measuring equipments. Hopefully, in the near future, the torque pulsations and Back-EMF will certainly be successfully measured and compared with both the analytical and numerical time-stepping FEM results.

Torque, flux and flux density values are in average value in Tables 1 and 2. Sensitivity analysis of both the PMDC and the FWDC motors are also considered. The results of FEM analysis and two-dimensional field distribution analytical method for different load conditions of the PMDC motor are compared in Table 2. The magnetic holders are devised to prevent the demagnetization of the permanent-magnets during the influence of a strong armature reaction field on the stator field. The FEM results have completely validated the operation of the holders during different load conditions. The sensitivity of the above mentioned output parameters to the variations of one permanent-magnet (PM) arc angle and its residual flux have also been successfully studied.

In this part, the results of FEM analysis are compared by the measured values of the prototypes. Fig. 7 through 10 show the efficiency and output power variations of the FWDC and PMDC motors, respectively. These results are compared with the measured efficiency and output power curves of the prototypes and they are in good agreements. Fig. 8 and Fig. 10 show the output characteristics of both FWDC and PMDC motors respectively, resulted from test and measurements of the motor variables. In Appendix 2, the whole measured variables and parameters of these two motors are shown in detail. Some other parameters such as starting torque, starting current and no-load torque are also predicted by both the time-stepping FEM and analytical method.

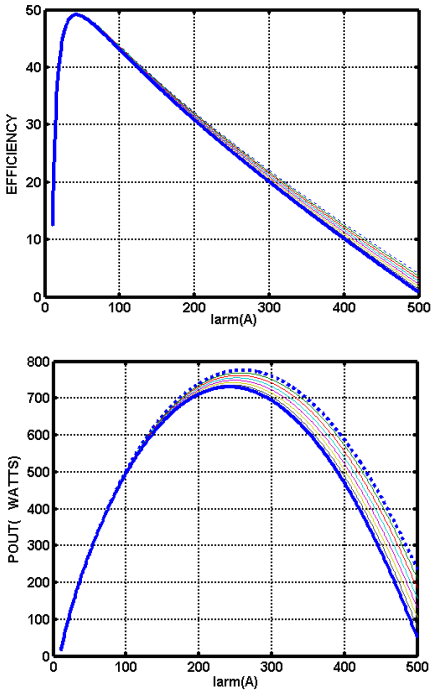

Fig. 7. Efficiency and output power [Watts]of the FWDC motor vs. line current [A]

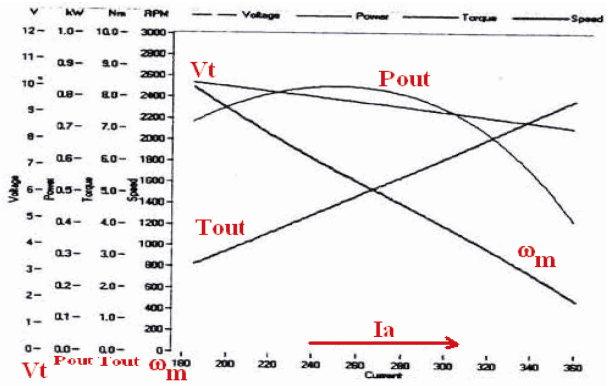

Fig. 8. Measured output power, torque and speed of the FWDC motor as a function of terminal voltage

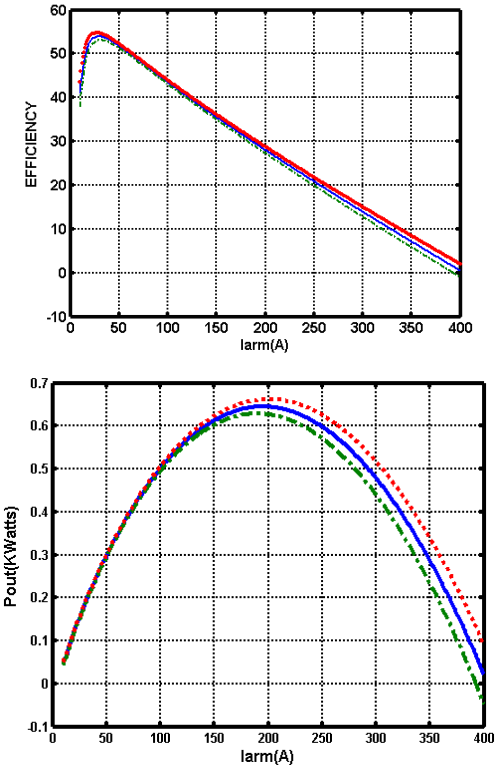

Fig. 9. Efficiency and output power [kWatts] of the PMDC motor vs. line current [A]

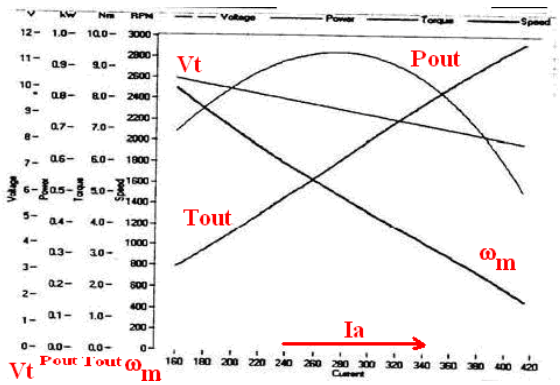

Fig. 10. Measured output power, torque and speed of the PMDC motor as a function of terminal voltage

Table 1. Comparison of FEM and analytical method results for the FWDC motor at load condition (they are average values of the waveforms)

	Time-stepping FEM	Analytical Method
$I_a = 150A$		
ω_m [RPM]	1747.9	1768
T_e [Nm]	0.533	0.529396
Φ_p [mWb]	1.1164	1.108
$B_{mid-aigap}$ [T]	1.13	1.1722
B_{Yoke} [T]	1.727	1.6212

Table 2. FEM and analytical method results for the PMDC motor at load condition (they are average values of the waveforms)

	Time-stepping FEM	Analytical Method
$I_a = 150A$		
ω_m [RPM]	1423.5	1780
T_e [Nm]	0.492	0.39
$E_{Coil-AVE}$ [V]	1.956	1.82
Φ_p [mWb]	0.4909	0.3923

5. Conclusion

In this paper, two previously-constructed prototypes, i.e., a permanent-magnet direct-current (PMDC) motor and a series-field-winding direct-current (FWDC) motor are compared from the output characteristics point of view. Results of an approximate analytical method, a previously-developed two-dimensional field analysis technique and time-stepping finite element method are compared for the prediction of airgap flux density distribution at the middle of the airgap of the motors, Back-EMF and electromagnetic torque produced in these two motors. The overall comparison of the results shows that this PMDC motor, which is smaller in mechanical size, can produce better electrical characteristics than the FWDC motor. The results of a few experimental measurements are also involved in this study and the results of all methods are also compared.

Acknowledgements

General acknowledgments to the Department of research and technology at the University of Isfahan.

Comments from the anonymous reviewers indeed helped to significantly improve the contents of this research. I

would really appreciate their comprehensive attentions and vital considerations.

Appendix 1

List of Symbols

α_m	Magnet arc angle
α_p	Pole-shoe arc angle
α'_p	Pole arc angle
P	Pole number

Appendix 2

PM and Field Winding DC Motor Parameter

PMDC Motor Data:

Stator

$D_{si} = 59.0mm$, $D_{so} = 79.0mm$,

$h_m = 7mm$, $\alpha_m = 35.19°mech$,

$B_r = 0.455T$, $H_c = -260\ KA/m$, $P = 6$

Rotor

$L_r = 60mm$, $D_{ri} = 38.6mm$,

$D_{ro} = 58.5mm$, $\omega_{slot} = 2.7mm$,

$D_{shaft} = 16.6mm$, $N_a = 116turns$

Field-Winding DC Motor Data:

Stator

$h_p = 8.6mm$, $D_{so} = 89.5mm$, $D_{si} = 78.2mm$

$\alpha_p = 68°mech$, $\alpha'_p = 37°mech$, $N_f = 8turns$,

$P = 4$, $A_{cond.} = 4.5*1.\ \ mm^2$

Rotor

$L_r = 48mm$, $D_{ri} = 60.5mm$, $D_{ro} = 39.0mm$

$D_{shaft} = 17.45mm$, $\omega_{slot} = 2.7mm$,

$\omega_{brush} = 5\ \ mm$, $l_{brush} = 10.\ \ mm$,

$N_a = 84turns$, $D_{cond.} = 2.1mm$

Stator lamination material* thickness=0.5 mm

Rotor lamination material* thickness=0.5 mm

* The stator and rotor lamination material characteristics were identified by measurements.

References

[1] J. J. Cathey, Electric machines, analysis and design, applying MATLAB, chapter 5, MCGRAW-HILL, 2001.

[2] N. Boules, "Prediction of no-load flux density distribution in permanent magnet machines," *IEEE Transactions on Industry Applications*, vol. IA-21, pp. 633-643, 1985.

[3] N. Boules, "Two-dimensional field analysis of cylindrical machines with permanent magnet excitation," *IEEE Transactions on Industry Applications*, vol. IA-20, pp. 1267-1277, September/October 1984.

[4] Z. Q. Zhu, D. Howe and C. C. Chan, "Improved analytical model for predicting the magnetic field distribution in brushless permanent–magnet machines," *IEEE Trans on Magnetics*, Vol. 38, no. 36, pp. 1010-1020, May 2002.

[5] Z. Q. Zhu, D. Howe, E. Bolte, and B. Ackermann, "Instantaneous magnetic field distribution in brushless permanent magnet DC motors, part I: Open-circuit field," *IEEE Trans. Magnetics*, vol.29, no.1, pp. 124-135, Jan.1993.

[6] Z. Q. Zhu and D. Howe, "Instantaneous magnetic field distribution in brushless permanent magnet DC motors, part II: Armature-reaction field," *IEEE Trans. Magnetics*, vol. 29, no. 1, pp. 136-142, Jan.1993.

[7] Z. Q. Zhu and D. Howe, "Instantaneous magnetic field distribution in brushless permanent magnet DC motors, part III: Effect of stator slotting," *IEEE Trans. Magnetics*, vol. 29, no. 1, pp. 143-151, Jan.1993.

[8] Z. Q. Zhu and D. Howe, "Instantaneous magnetic field distribution in brushless permanent magnet DC motors, part VI: Magnetic field on load," *IEEE Trans. Magnetics*, vol. 29, no. 1, pp. 152-158, Jan.1993.

[9] Z. Q. Zhu and D. Howe and Z. P. Xia, "Prediction of open-circuit airgap field distribution in brushless machines having an inset permanent magnet rotor topology," *IEEE Trans. Magnetics*, vol. 30, no. 1, pp. 98-107, Jan.1994.

[10] M. Cheng, et al., "Nonlinear varying-network magnetic circuit analysis for doubly salient permanent-magnet motors", *IEEE Trans. on Magnetics*, vol. 36, no. 1, pp. 339-348, January 2000.

[11] A. Kioumarsi, M. Moallem and B. Fahimi, "Mitigation of torque ripple in interior permanent magnet motors via optimal shape design," *IEEE Trans. on Magnetics*, pp. 3706-3711, November 2006, IEEE, 2006.

[12] A. Kiyoumarsi, M. Hassanzadeh and M. Moallem, "A new analytical method on field calculation for interior permanent-magnet synchronous motors," *International Journal of Scientia Iranica, Sharif University of Technology*, vol. 13, no. 14, pp. 364-372, October 2006.

[13] A. Kiyoumarsi, Shape design optimization of the rotor of an interior permanent-magnet synchronous motor, *PhD thesis, Isfahan University of Technology*, Isfahan, Iran, 2004.

[14] A. Kiyoumarsi et al., FINITE ELEMENTS, Book published by *WSEAS Press*, Chapter 12, Application of the Finite Element Method in Design and Analysis of Permanent-magnet Motors, pp. 138-152, August 2007.

[15] A. Kiyoumarsi, A., Optimal Shape Design, Construction and Testing of an Interior Permanent-Magnet Synchronous Motor, Institute of Electrical Machines, *Berlin University of Technology*, Berlin, *Post-Doctoral Research Report*, August 2007.

Arash Kiyoumarsi He was born in Shahr-e-Kord, Iran, on September 11th, in the year 1972. He received B.Sc. (with honors) from Petruliom University of Technology (PUT), Iran, in electronics engineering in 1995 and M.Sc. from Isfahan University of Technology (IUT), Iran, in electrical power engineering in 1998. He received Ph.D. degree from the same university in electrical power engineering in 2004. In March 2005 he jointed to the University of Isfahan, Faculty of Engineering, Department of Electrical Engineering as an assistant professor. He was a Post-Doc. research fellow of the Alexander von Humboldt foundation at the Institute of Electrical Machines, Technical University of Berlin from February to October 2006 and July to August 2007. His research interests have included application of finite element analysis in electromagnetics, interior permanent-magnet synchronous motor drives, shape design optimization and nonlinear control of electrical machines. (Department of Electrical Engineering, Faculty of Engineering, University of Isfahan, Iran, Phone: +98 311 7934018, Fax: +98 311 7933071, Postal code: 81746-73441, E-Mails: kiyoumarsi@eng.ui.ac.ir , kiyoumarsi_arash@yahoo.com.)